INFRARED FIBERS IN THE 1.5 μm TO 18 μm RANGE: AVAILABILITY AND MEASURED PROPERTIES

Robert Felkel, Walter Leeb

Vienna University of Technology, Institute of Communications and Radio-Frequency Engineering, Gusshausstrasse 25/389, 1040 Vienna, Austria, Email: rfelkel@nt.tuwien.ac.at

ABSTRACT

With a view towards the application in space-borne optical instruments, we first performed a world-wide market survey of infrared fibers designed for the wavelength range of 1.5 μm to 18 μm. Fiber samples purchased and tested comprise fluoride fibers, chalcogenide fibers, a germanate fiber and a silver-halide fiber, as well as hollow fibers. While the majority of infrared fibers offered are of the multi-mode type, three of the fluoride fibers are single-mode. We report on the polarization degrading effect of a single-mode fiber and present a possible solution to achieve polarization maintainance by twisting the fiber. Secondly we report on measurements of numerical aperture, output beam profile, and attenuation of a hollow fiber. The measurements were performed at the wavelengths of $\lambda = 3.39\,\mu$m and $\lambda = 10.6\,\mu$m.

1. INTRODUCTION

Infrared fibers designed for the wavelength range of 1.5 μm to 18 μm may take over several functions in space-borne optical instruments replacing conventional bulk optics. Fiber solutions may increase flexibility and simplicity, decreasing system size and weight at the same time. Multi-mode fibers can be used for transmitting power, without regard of the optical phase. Possible applications for these fibers can be found in classical imaging and in spectroscopy. Other, more sophisticated applications rely on preserving phase (or even polarization) and thus ask for single-mode fibers. In this context, important applications could be optical path length control and beam guidance in phased antenna arrays, as well as modal wavefront filtering in nulling interferometry.

2. TYPES OF INFRARED FIBERS

The largest and most common group of infrared fibers are *solid core fibers*. They consist of a core surrounded by a cladding with a slightly lower refractive index. The principle of light guiding is total internal reflection. Solid core fibers can be classified into *glass fibers* and *crystalline fibers*. Depending on the material, glass fibers are divided into *heavy metal fluoride glass fibers* transmitting from below 1 μm up to about 4 μm, *germanate glass fibers* transparent from 1 to 3 μm, and *chalcogenide glass fibers* usable from about 2 μm up to 10 μm. Crystalline fibers can be further divided into *single-crystal fibers* which mainly use sapphire (Al_2O_3) as host material, transmitting from 0.5 to 3.2 μm and *polycrystalline fibers* that are manufactured by an extruding process. Within this subgroup silver-halide fibers are most important, transmitting from about 3 μm up to 18 μm.

A second group of infrared fibers are *hollow fibers*. They propagate light in a hollow core enclosed either by a metallic film or by a material with a refractive index < 1, e.g. sapphire near 10 μm. Hollow fibers of the first type, the so-called *leaky guides*, rely on the reflectivity of metallic surfaces, whereas the guiding mechanism of the second type is the same as in standard solid core fibers. Hollow metallic fibers provide a wide transmission range from 3 to 12 μm.

A third group, *photonic crystal fibers*, take advantage of so called photonic crystals. They rely on periodic microstructures in one, two or three dimensions. At present, these fibers are intensively researched but not commercially available in the mid-infrared.

3. GLOBAL MARKET SURVEY

We performed a word-wide market survey concerning optical fibers in the mid-infrared spectral range from 1.5 μm to 18 μm. Manufacturers and distributors for various types of fibers were contacted and we asked for offers and detailed specifications. Based on the results of this survey, we selected potentially interesting fibers and ordered fiber samples with lengths from 2 to 5 m. Tab. 1 summarizes the purchased test samples, listing type, core diameter, wavelength range and mode property (single-mode / multi-mode). Some of the fibers described in Section 2 were not commercially available yet. Only fluoride fibers were available as single-mode fibers. We took the numerical aperture and the core diameter specified by the

Proc. '6th Internat. Conf. on Space Optics', ESTEC, Noordwijk, The Netherlands, 27-30 June 2006 (ESA SP-621, June 2006)

Tab. 1. Purchased fiber test samples. The abbreviations SM and MM denote single-mode fiber and multi-mode fiber, respectively.

material/ type	product designation	core diameter [μm]	wavelength range [μm]	fiber type
fluoride	SMFF	8.5	$0.5-3.7$	SM
	SMFF	10	$0.5-3.7$	SM
	TFF	190	$0.7-2.5$	MM
	GFF	160	$0.5-4$	MM
	SG	100	$0.45-5$	MM
	MIDIRMM	62.5	$0.3-4.5$	MM
	MIDIRSM	9	$0.3-4.5$	SM
germanate	HP	250	$1-3$	MM
chalco-	C1	250	$2-10$	MM
genide	CIR	215	$1.5-6$	MM
silver-halide	SPGR	900	$3-18$	MM
hollow	HWEA	300	$2.9-12$	MM
	HWCA	300	$2.9-12$	MM
	HITACHI	700	$3-12$	MM

manufacturer to calculate the cut-off wavelength λ_c and obtained $\lambda_c = 2.3\,\mu$m and $\lambda_c = 2.7\,\mu$m for the fibers SMFF with 8.5 μm and 10 μm core and an upper boundary of $\lambda_c = 3.5\,\mu$m for fiber MIDIRSM.

4. EXPERIMENTAL RESULTS

4.1. Single-Mode Fluoride Fiber

As a representative for a single-mode fiber, we tested the fluoride fiber SMFF with 8.5 μm core diameter using a HeNe laser at the wavelength $\lambda = 3.39\,\mu$m. For input coupling we used an AR-coated zinc-selenide meniscus lens with 14.5 mm focal length. The laser emmitted a lineary polarized, Gaussian-shaped beam with a $1/e^2$-beam diameter of 4.5 mm. The fiber sample was 281 cm long. With an eye towards possible applications in phased antenna arrays we investigated the influence of the fiber on the light's state of polarization (SOP).

4.1.1. Measurement of Birefringence

We performed two birefringence measurements applying the twisting methods according to Okoshi [1] and Huang [2]. Okoshi's method simply measures the state of polarization (SOP) of the light after passing the fiber for various fiber twist angles. Huang's method relys on a more extensive nulling scheme involving the polarization eigenmodes of twisted single-mode fibers. Both methods produce (different) measurement curves that allow to determine the linear birefringence $\Delta\beta$ of the investigated fiber, being the difference of the propagation constants along the fast and slow axis. It was shown in [1, 2], that the measurement curves are symmetric, provided that the fiber is homogenous over the fiber length (i.e. neither the linear birefringence $\Delta\beta$ nor the axes of linear birefringence change over the fiber length). However, the measurement curves we obtained in the laboratory did not show the expected symmetry which indicates that the fluoride fiber tested is not homogenous. Hence a reliable determination of $\Delta\beta$ is not possible using the twisting methods.

In a next step we simulated measurement curves underlying an inhomogenous fiber model. The inhomogenous fiber consisted of several homogenous fiber sections with different orientation of the birefringence axes. The simulations approved the expected unsymmetry of the measurement curves for inhomogenous fibers and could qualitatively explain our laboratory results.

The findings in the laboratory combined with experience from the simulations indicate that the investigated fluoride fiber is weakly birefringent with a beat length larger than one meter (the beat length L_B is related to birefringence $\Delta\beta$ by $L_B = 2\pi/\Delta\beta$), but the axes of birefringence change statistically over the fiber length on a scale smaller than the beat length. Consequently also the state of polarization changes statistically within the fiber.

4.1.2. Polarization Maintaining by Fiber Twisting

We showed in Section 4.1.1 that the state of polarization (SOP) changes statistically within the fiber. On the other hand, phased antenna arrays critically rely on a well defined SOP. One possible solution to overcome this problem is to preserve the SOP by twisting the fiber. In a sufficiently strong twisted single-mode fiber the linear birefringence $\Delta\beta$, being of statistical nature, can be neglected compared to the circular birefringence caused by the fiber twist. This circular birefringence is well defined because it depends only on the twist for a given fiber and is moreover homogenous when the elasticity of the fiber is constant over the length. Circular birefringence causes only a rotation of the polarization plane, thus the state of polarization in front of the fiber is preserved except for a certain rotation. The OHANA [3] project has taken advantage of this effect, aiming to realize a near-infrared interferometer based on silica and fluoride fiber technology.

In the laboratory we have used the setup shown in Fig. 1 to demonstrate the polarization maintaining effect. A quarterwave plate was used to generate various SOPs at the fiber input. Depending on the rotation angle α of the quarterwave plate the beam emitted by the laser with linear SOP along the x-axis was transformed into elliptically polarized light of various ellipticity. We determined the

SOP in terms of azimuth angle ψ, being the direction of the main axis of the polarization ellipse with respect to the laboratory coordinate system (x,y), and of ellipticity $\epsilon = \mathrm{b/a}$ defined as ratio of field amplitudes in the main axes of the polarization ellipse (see Fig. 2).

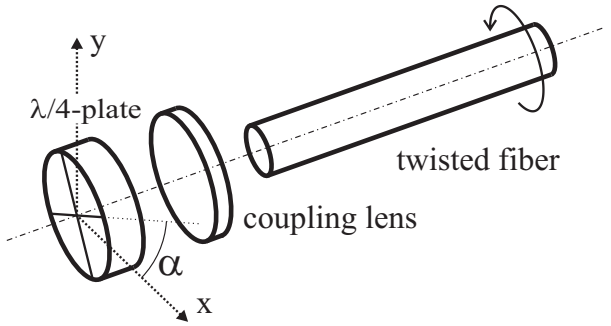

Fig. 1. Setup for measurement of state of polarization (SOP) with twisted fibers. The SOP behind the fiber was compared to the calculated SOP behind the $\lambda/4$-plate, i.e. at the fiber input. Depending on the rotation angle α of the $\lambda/4$-plate various SOPs were generated from the incident light polarized in x-direction.

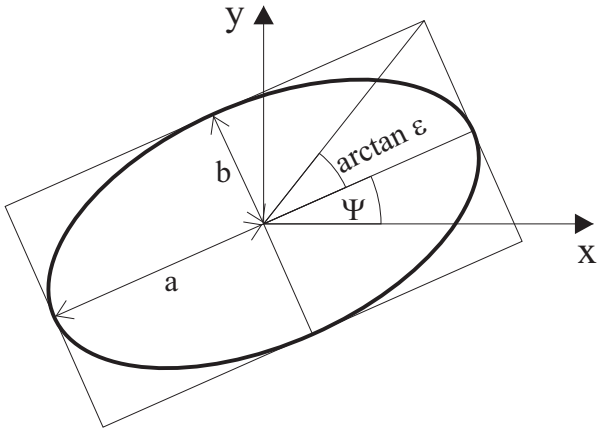

Fig. 2. Determination of state of polarization in terms of ellipticity $\epsilon = \mathrm{b/a}$ and azimuth angle ψ of the polarisation ellipse. The axes x and y denote a laboratory coordinate system.

We measured the SOP behind the fiber for various rotation angles α and compared it to the SOP at the fiber input. The SOP at the input was calculated, assuming a perfect quarterwave plate. The results for the untwisted fiber (see Fig. 3) show that the fiber seriously degrades the state of polarization. We repeated the same measurement with the fiber twisted with five $360°$-twists per meter. The results given in Fig. 4 show good agreement of input and output SOP, confirming the polarization maintaining effect of twisting. We also observed the expected rotation of the polarization plane, which was $156°$ plus an unknown multiple of $180°$ in the specific case. (The rotation of the polarization plane causes an offset of azimuth ψ in Fig. 4 which has been suppressed to get congruent curves.)

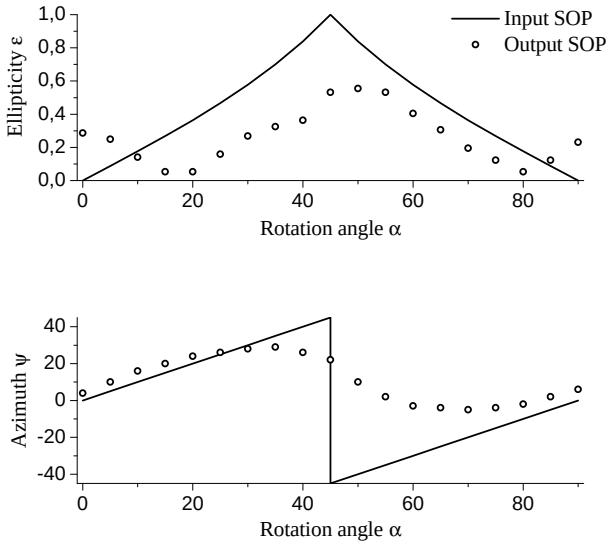

Fig. 3. Change of state of polarization (SOP) caused by a piece of untwisted fiber SMFF.

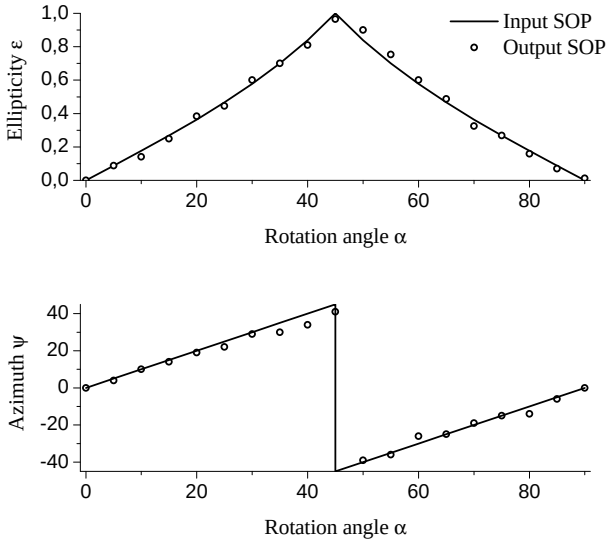

Fig. 4. States of polarization (SOP) in front of and behind fiber SMFF twisted with five $360°$-twists per meter. As evident, the fiber maintains the SOP when twisted.

4.2. Hollow Fiber

Unexpected results have also be obtained with the hollow fiber HWEA which has a core diameter of $300\,\mu$m. We have measured the effective numerical aperture, the output intensity disribution and the attenuation (also vs. bending radius) with a HeNe laser at $\lambda = 3.39\,\mu$m and with a CO_2 laser at $\lambda = 10.6\,\mu$m. Fiber HWEA has been developed for Er:YAG lasers ($\lambda = 2.94\,\mu$m), so we expected less attenuation at $3.39\,\mu$m.

For measurements at $\lambda = 3.39\,\mu$m we used a zinc-selenide meniscus lens with focal length $f = 8.3$ cm for coupling light into the fiber. The laser beam diameter at the coupling lens was 4.5 mm. A pyroelectric detector array was used to measure the fiber's output beam profile at various distances from the fiber facet. Fig. 5 shows the beam profile 30 mm behind the fiber. The total displayed area in the figure is $12.4 \times 12.4\,\text{mm}^2$. When the fiber is slightly bent the output field distribution changes, as expected for multi-mode fibers. The measured intensity distribution indicates that low order modes are excited predominantly. From the beam profiles we determined the effective numerical aperture to be $\text{NA}_{\text{eff}} = 0.0096$, defined by an intensity drop to 5% of peak intensity. This rather small value is consistent with theory [4] and is typical for hollow fibers because of their large core diameter.

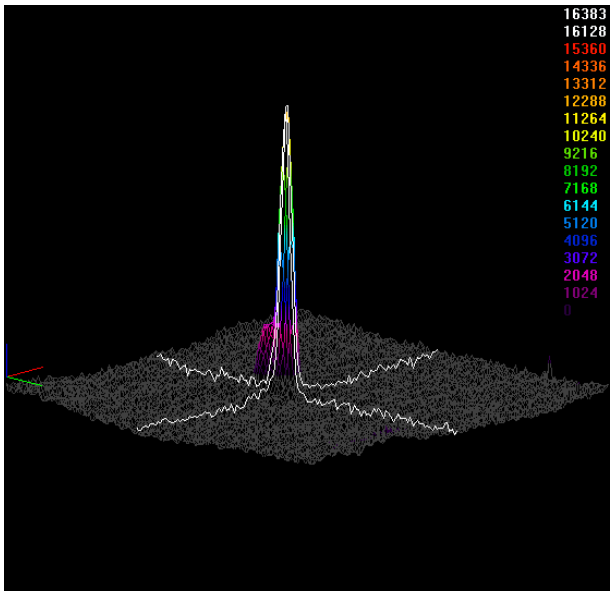

Fig. 5. Output intensity distribution of the HWEA hollow fiber at $\lambda = 3.39\,\mu$m, measured 30 mm behind the fiber facet. The total displayed area is $12.4 \times 12.4\,\text{mm}^2$. Low order modes are excited predominantly.

We determined the insertion loss of the HWEA fiber using a 263 cm long fiber sample straightened over its entire length. We placed a pinhole with a diameter equalling the fiber's core (300 μm) directly in front of the fiber facet. The power at the fiber output was determined with an indium antimonide (InSb) photovoltaic detector and compared it to the power measured directly behind the pinhole. We obtained an insertion loss of 6.5 dB. This figure includes the fiber attenuation as well as the coupling loss.

To measure the influence of bending on attenuation we wrapped the fiber partly onto a mandrel. Two effects seem to contribute to the bending-induced attenuation: The pure bending loss increases with smaller bending radius (keeping the bent length constant) as expected, leading to a floor value of bending-induced loss. However, as a second influence we observed that applying additional minor bends (along a small length and with large radius of bending compared to the bending due to wrapping onto the mandrel) can lead to strong additional loss. This behaviour may be explained by power coupling into higher order modes at these minor bends, which modes are strongly attenuated in hollow fibers. Fig. 6 shows the bending-induced attenuation vs. bending radius. At each radius three turns of fiber have been wrapped onto the mandrel. We applied additional minor bends to the fiber and measured the maximum and minimum loss for each radius. A single minor bends typically increased the bending-induced loss by up to 2 dB.

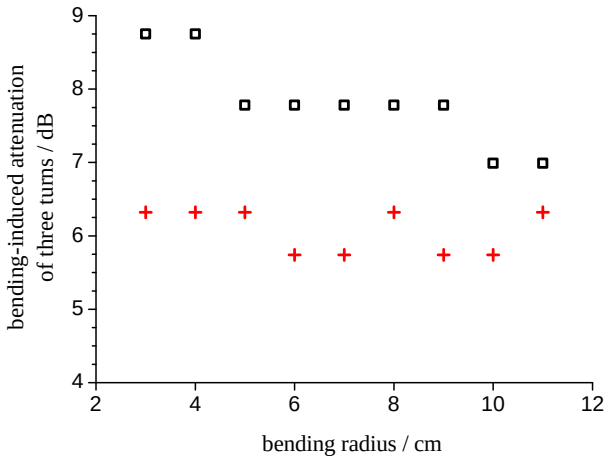

Fig. 6. Maximum (squares) and minimum (crosses) bending loss at $\lambda = 3.39\,\mu$m of three turns of HWEA hollow fiber for various bending radii when an additional minor bend was applied.

We repeated the same measurements at $\lambda = 10.6\,\mu$m using a zinc-selenide meniscus lens with a focal length $f = 1.75$" for input coupling. The laser beam was Gaussian-shaped with a beam diameter of 5.2 mm at the coupling lens. Again the pyroelectric detector array was used to measure the fiber's output beam profile at various distances from the fiber facet. The intensity distribution 20 mm behind the fiber facet is shown in Fig. 7. The beam profile is "donut"-shaped. When the fiber was bent, the intensity distribution changed, but the central minimum always remained. Changing the launch conditions using various coupling lenses with focal lengths between 1.25" and 5" did not lead to an excitation of the fundamental mode as one would expect. The effective numerical aperture was found to be $\text{NA}_{\text{eff}} = 0.06$. This value is about six times the one obtained at $\lambda = 3.39\,\mu$m. It can be explained partly by the longer wavelength and partly by the higher order mode that is excited predominantly. Again the obtained value is in good agreement with [4].

Using a CdHgTe photovoltaic detector we measured the insertion loss of the hollow fiber HWEA at $\lambda = 10.6\,\mu$m. For the 263 cm long straigthened fiber we obtained a value of 9.8 dB, including both fiber attenuation and coupling loss. Figure 8 shows the bending-induced attenuation of three turns of fiber for various radii of bending.

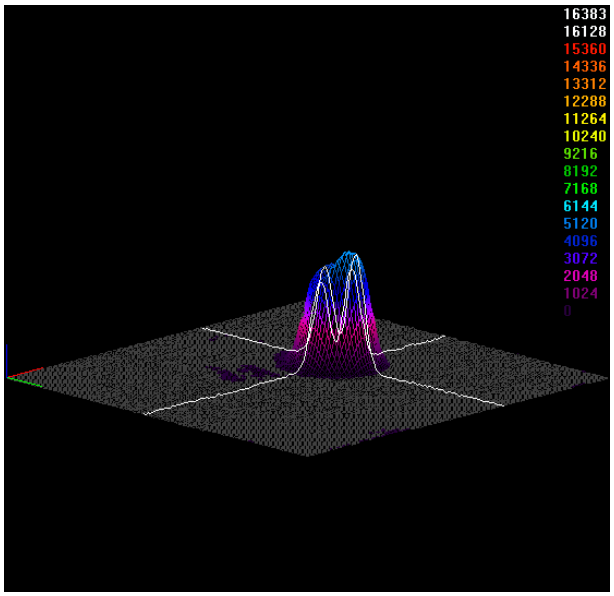

Fig. 7. Output intensity distribution of the HWEA hollow fiber at $\lambda = 10.6\,\mu$m, measured 20 mm behind the fiber facet. The total displayed area is $12.4 \times 12.4\,\text{mm}^2$. The beam is "donut"-shaped.

Again, the observed maxima and minima were caused by a single additional minor bend typically increasing the bending-induced loss by up to 6 dB.

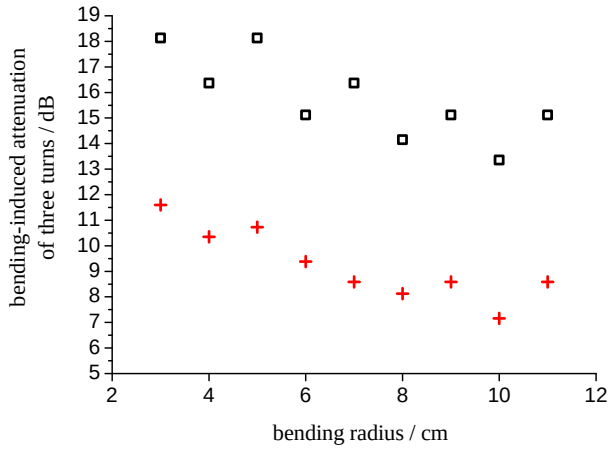

Fig. 8. Maximum (sqares) and minimum (crosses) bending loss at $\lambda = 10.6\,\mu$m of three turns of HWEA hollow fiber for various bending radii when an additional minor bend was applied.

5. SUMMARY

The majority of commercially available infrared fibers are of the multi-mode type. Only fluoride fibers, transmitting in the range of 0.5 μm to about 4 μm are available as single-mode fibers.

The applicability of infrared fibers may be restricted by polarization degrading effects. We showed, for a fluoride single-mode fiber operated at $\lambda = 3.39\,\mu$m, that twisting the fiber preserves the state of polarization of transmitted light. This may allow to use these fibers in phased antenna arrays.

In a hollow multi-mode fiber, apart from the expected increase of attenuation with decreasing bending radius, we could observe a strong dependence of transmitted power on minor bends. This additional loss was found to be typically up to 2 dB at $\lambda = 3.39\,\mu$m and up to 6 dB at $\lambda = 10.6\,\mu$m.

REFERENCES

[1] T. Okoshi, S. Ryu, and K. Emura, Measurement of polarization parameters of a single-mode optical fiber. *Journal of Optical Communications*, Vol. 2, pp. 134-141, 1981.

[2] S. Huang and Z. Lin, Measuring the birefringence of single-mode fibers with short beat length or nonuniformity: a new method. *Applied Optics*, Vol. 24, No. 15, pp. 2355-2361, 1985.

[3] G. Perrin, O. Lai, J. Woillez, J. Guerin, T. Kotani, S. Vergnole, A. J. Adamson, C. Ftaclas, O. Guyon, P. Lena, J. Nishikawa, F. Reynaud, K. Roth, S. T. Ridgway, A. T. Tokunaga, and P. L. Wizinowich, OHANA. *New Frontiers in Stellar Interferometry, Proceedings of SPIE*, Vol. 5491, paper 5491-43, 2004.

[4] R. Nubling and J. A. Harrington, Launch conditions and mode coupling in hollow glass waveguides. *Optical Engineering*, Vol. 37, No. 9, pp. 2454-2458, 1998.